STEM CELLS AND DEVELOPMENT
Volume 00, Number 00, 2024
© Mary Ann Liebert, Inc.
DOI: 10.1089/scd.2024.0105

Open camera or QR reader and
scan code to access this article
and other resources online.

Modeling Choroideremia Disease with Isogenic Induced Pluripotent Stem Cells

Ana Fragoso Fonseca,[1] Rita Coelho,[1] Mafalda Lopes-da-Silva,[1] Luísa Lemos,[2] Michael J. Hall,[1] Daniela Oliveira,[1] Ana Sofia Falcão,[1] Sandra Tenreiro,[1] Miguel C. Seabra,[1,2] and Pedro Antas[1,2]

Choroideremia (CHM) is a rare X-linked chorioretinal dystrophy causing progressive vision loss due to mutations in the *CHM* gene, leading to Rab escort protein 1 loss of function. CHM disease is characterized by a progressive degeneration of the choroid, the retinal pigment epithelium (RPE), and the retina. The RPE is a monolayer of polarized cells that supports photoreceptors, providing nutrients, growth factors, and ions, and removes retinal metabolism waste products, having a central role in CHM pathogenesis. Commonly used models such as ARPE-19 cells do not reproduce accurately the nature of RPE cells. Human induced pluripotent stem cells (hiPSCs) can be differentiated into RPE cells (hiPSC-RPE), which mimic key features of native RPE, being more suited to study retinal diseases. Therefore, we took advantage of hiPSCs to generate new human-based CHM models. Two isogenic hiPSC lines were generated through CRISPR/Cas9: a CHM knock-out line from a healthy donor and a corrected CHM patient line using a knock-in approach. The differentiated hiPSC-RPE lines exhibited critical morphological and physiological characteristics of native RPE, including the presence of the tight junction markers Claudin-19 and Zonula Occludens-1, phagocytosis of photoreceptor outer segments, pigmentation, a postmitotic state, and the characteristic polygonal shape. In addition, all the studied cells were able to form retinal organoids. This work resulted in the establishment of isogenic hiPSC lines, representing a new and important CHM cellular model. To our knowledge, this is the first time that isogenic cell lines have been developed to model CHM disease, providing a valuable tool for studying the mechanisms at the onset of RPE degeneration.

Keywords: choroideremia, CRISPR/Cas9, human induced pluripotent stem cells, retinal pigment epithelium

Introduction

Choroideremia (CHM) is a chorioretinal dystrophy marked by progressive degeneration of the choroid, retinal pigment epithelium (RPE), and photoreceptors (PR). Symptoms begin in the first decade of life, with male patients experiencing nyctalopia, followed by peripheral vision loss and complete blindness in late adulthood. This X-linked recessive disease is caused by *CHM* gene mutations, which encode for Rab escort protein 1 (REP1). REP1 is required for the prenylation of Rab GTPase proteins and their transport to target membranes, which are essential for vesicle trafficking in the endocytic and exocytic pathways.[1–5]

Loss of REP1 can be compensated in most tissues by its isoform REP2 (encoded by CHM-like gene, *CHML*), which shares 75% sequence identity and is also ubiquitously expressed.[5–7] However, in the retina, it seems that some key Rab proteins have less affinity for REP2, leading to the accumulation of unprenylated Rab and an exclusive eye phenotype.[2,5,8] REP1 absence in RPE cells is thought to affect opsin transfer to photoreceptor outer segments (POS), apical distribution of melanosomes, and POS phagocytosis, yet the processes underlying CHM degeneration are still not well understood.[2]

The RPE is a monolayer of polarized cells that supports the PR, performing several essential functions such as providing nutrients, growth factors, and ions to the PR, while eliminating waste products from retinal metabolism.[9–11] Furthermore, RPE cells perform daily phagocytosis of POS and contribute to inflammatory signaling.[10]

[1]iNOVA4Health, NOVA Medical School | Faculdade de Ciências Médicas, NMS | FCM, Universidade Nova de Lisboa, Lisboa, Portugal.
[2]Champalimaud Research, Champalimaud Foundation, Lisbon, Portugal.

Multiple retinal dystrophies impair RPE function, resulting in vision loss[11]; thus, several RPE models are currently routinely used. ARPE-19 (Adult Retinal Pigment Epithelial cell line-19) is one of the most used cell lines to study retinal diseases because of its simplicity and availability. Although this cell line has some advantages, such as being readily available commercially and having good viability and proliferation properties in culture, it is now clear that it has some limitations regarding its relevance and data reproducibility.[12] Because ARPE-19 immortalization occurred spontaneously, these cells exhibit replicative exhaustion and senescence, as well as chromosomal aberrations, as the number of passages increases.[12,13] In addition, ARPE-19 cells produce some RPE-specific mRNA transcripts without the corresponding protein expression, such as RPE65, BEST1, and CLDN19, leading to an incompletely differentiated phenotype. Regarding pigmentation, most studies report absent or heterogeneous melanin accumulation in ARPE-19, which, on top of an incomplete protein network supporting the activity of junctional complexes, do not represent accurately the physiological functionality of a complete monolayer.[12]

In a study by Markert and colleagues, the authors compared the transcriptional profile between various RPE sources, including adult human primary RPE (ahRPE), human induced pluripotent stem cell (hiPSC)-derived RPE, and ARPE-19, to investigate differences in aging, maturation, and plasticity.[14] They observed that ahRPE and hiPSC-RPE shared a similar RPE gene expression profile, while ARPE-19 had a significantly lower RPE signature gene expression profile, consistent with a reduced transepithelial electrical resistance (TEER).[14]

Given the limitations of ARPE-19 usage, it is of high interest to develop more relevant and robust models to study retinal diseases.[12] The use of hiPSC-derived RPE (hiPSC-RPE) models may help study and understand various retinal disorders as they can offer an unlimited supply of RPE for cell therapies and are already used in multiple clinical trials.[11]

The development of cellular disease models from individual patients was made possible with hiPSC technology, enabling the study of genetic alterations in various cell types. This, coupled with advances in genome editing techniques such as the clustered regularly interspaced short palindromic repeat (CRISPR) system, allows the repair of causative alleles in patient cell lines or the introduction of disease alleles into healthy cell lines. Together, this permits the investigation of isogenic cell pairs varying in a single genetic change, enabling research into the molecular and cellular phenotypes underlying specific mutations.[15]

In this study, we developed two isogenic cell lines using CRISPR/Cas9 to model CHM disease, from two different sources: a healthy donor cell line (RBi001-A) and a patient-derived hiPSC line (CRFi001-A). Moreover, we demonstrate that these cells can differentiate into RPE and show typical RPE morphological and molecular characteristics.

The development of these isogenic lines is a valuable contribution for CHM research since it provides a reliable platform for further investigating the pathological mechanisms underlying this degenerative disease.

Materials and Methods

hiPSC culture

hiPSC lines were cultured according to the StemFlex™ medium (#A3349401, Gibco™) user guide, on 6-well plates (#3506, Corning®) precoated with 20 μg cm^{-2} of Growth Factor Reduced Matrigel (GFR, #354230, Corning®). When 80% confluence was reached, the hiPSCs were subcultured for expansion or experimental use, using Versene Solution (#15040066, Gibco™) at a ratio between 1:2 and 1:4 in StemFlex™ medium and maintained at 37°C in a humidified atmosphere containing 5% CO_2.

Gene editing of hiPSCs

In this study, we generated two cell lines by genome editing. First, we used a healthy hiPSC line, RBi001-A (#66540025, ECACC), to produce a *CHM* knock-out (KO) line (Strategy 1). Next, we used a CHM male patient-derived hiPSC line, CRFi001-A, which was kindly provided by David Gamm Lab (Wisconsin University), where we corrected the mutation (Strategy 2). This cell line harbors a *CHM* gene mutation in a single nucleotide at c.808C>T, leading to an early stop codon. The cell lines used are hereafter referred to as RBi CHM+ (healthy donor control) and RBi CHM– (isogenic KO), and Pt CHM– (patient cell line) and Pt CHM+ (isogenic corrected line).

We designed single guide RNAs (sgRNAs) for gene editing using the CRISPOR (http://crispor.tefor.net/) online tool. On both strategies, the sgRNAs target CHM exon 6 (5′-TGCATTTCGAGAAGGACGAGTGG-3′; 5′-TGCATTTCGAGAAGGATGAGTGG-3′—Strategy 1 and 2, respectively). However, on Strategy 2, in addition to the sgRNA, whic targets the mutation, a single-stranded oligodeoxynucleotide (ssODN) 5'-AATCAAATCTAATGTTAGTCGATATGCAGAGTTTAAAAATATTACCAGGATTCTTGCATTTCGAGAAGGACGAGTGGAACAGGTTCCGTGTTCCAGAGCAGATGTCTTTAATAGCAAACAACTTACTATGGTAGAAAAGC-3′ was used to induce the homology-directed repair (HDR) mechanism and correct the CHM mutation on CRFi001-A cells.

The two hiPSC lines were generated using CRISPR/Cas9 components following the Lipofectamine™ Stem Transfection Reagent (#STEM00001, Invitrogen™) protocol. Briefly, one day before transfection, cultures with <85% confluence were seeded as single cells, using approximately 75 000 cells/well, in 24-well plates (#3524, Corning®) precoated with 2 μg cm^{-2} of Biolaminin 521 LN (#LN521-05, BioLamina). The next day, wells with ∼30% confluence were transfected using Lipofectamine™ Stem Transfection Reagent (#STEM00001, Invitrogen™), as per manufacturer's instructions. For *CHM* KO, RBi001-A cells were incubated for 4 h with 500 ng sgRNA and 1.5 μg Cas9 ribonuclease protein (RNP) complex (TrueCut™ Cas9 Protein v2, #A36496, Invitrogen™). To correct the *CHM* mutation in CRFi001-A cells, the RNP complex contained an additional 10 μM of ssODN template. Then, before reaching 85% confluence, hiPSCs were passaged and further sorted into 96-well (#3997, Corning®) Matrigel-coated plates at 1 cell/well, to ensure clones obtained from isolated colonies. Colonies

were allowed to expand, and positive clones were confirmed by Western Blot (WB) and Sanger sequencing.

hiPSC-RPE differentiation

hiPSCs were grown as described previously, and differentiation into RPE was induced using Foltz LP et al.'s[11] method, by sequential addition of growth factors for 14d in Retinal Differentiation Medium (RDM). On d14, immature RPE was collected and plated at $\sim 1x10^5$ cells cm^{-2} on laminin-coated 6-well plates (passage 0, P0) and were allowed to mature in X-VIVO (TheraPEAK™ X-VIVO™–10, #BP04-743Q, Lonza) containing 1% Antibiotic-Antimycotic (AB/AM, #15240062, Gibco™), which was changed twice per week. On d30, when pigmentation was visible, the cells were further expanded to P1 and matured roughly 30d later, at which point, they were used for experiments (from P1 to P4).

Retinal organoid differentiation from hiPSCs

Retinal organoid (RO) differentiation was carried out according to Capowski EE et al.'s[16] protocol with slight alterations. Briefly, hiPSCs at 80% confluence were lifted using Versene and split at 3000 cells/well in a Nunclon™ Sphera™ 96-Well U-Shaped-Bottom Microplate (#174925, Thermo Scientific™) using StemFlex™ medium supplemented with 10 μM of Rho-associated protein kinases inhibitor (Y-27632, #10–2301, Focus Biomolecules). The cells were grown as embryoid bodies (EBs) for 7d, doing an adaptation to Neural Induction Medium (NIM) containing Dulbecco's Modified Eagle Medium/Nutrient Mixture F-12 (DMEM/F-12, #10565018, Gibco™), 1% N-2 supplement (#17502048, Gibco™), 1X Non-Essential Amino Acids Solution (NEAA, #11140050, Gibco™), 1X GlutaMAX™ Supplement (#35050038, Thermo Scientific™), and 2 mg/ml Heparin (#H3149, Sigma-Aldrich®). On d6, 1.5 nM of Bone Morphogenetic Protein-4 (#120-05, PeproTech®) was added to fresh NIM, and on d7 EBs were transferred to GFR Matrigel-coated 6-well plates to allow optic cup formation. The medium was replaced by half fresh NIM on d9, 12, and 15. On d16, the medium was replaced by RDM containing DMEM: F12 (3:1), 2% B-27™ minus vitamin A (#12587010, Gibco™), 1X NEAA, 1X GlutaMAX™, and 1X AB/AM and changed every 2 days. On d30, optic vesicles were manually dissected using a surgical scalpel (SM65A, Swann-Morton® Ltd) under the microscope EVOS™ XL Core (ThermoFisher Scientific). After dissection, organoids were cultured in suspension in 3D retinal differentiation medium (3D-RDM) containing DMEM:F12 (3:1), 2% B-27 minus vitamin A, 1X NEAA, 1X GlutaMAX™, 1X AB/AM, 5% Fetal Bovine Serum (FBS, #A5256801, Gibco™), 1:1000 Chemically Defined Lipid Concentrate (#11905031, Gibco™), and 100 μM Taurine (#T8691, Sigma-Aldrich®) and supplemented with 1 μM of all-*trans*-Retinoic acid (RA, #R2625, Sigma-Aldrich®) until d100. After this point, organoids were maintained in 3D-RDM without RA to enhance maturation of PR. Brightfield images were acquired at differentiation d3, 7, and 140.

Western blotting

hiPSC or hiPSC-RPE was lysed on ice with Cell Lysis Buffer (#9803, Cell Signaling Technology®) containing Halt™ Protease and Phosphatase Inhibitor Cocktail (#78444, Thermo Scientific™) diluted to 1X. Pierce™ BCA Protein Assay Kit (#23225, Thermo Scientific™) was used to determine protein concentrations and 8% polyacrylamide gels were loaded with 30 μg of protein lysate, previously denaturated at 95°C for 5 min. Gels were then transferred onto 0.2 μm nitrocellulose membranes using Bio-rad Trans-Blot Turbo Transfer System. The following primary antibodies were used at the indicated dilutions: REP1 (#AB0123, SICGEN, 1:500), REP2 (#AB0132, SICGEN, 1:500), Oct3/4 (#sc-5279, Santa Cruz Biotechnology, 1:500), Nanog (#sc-134218, Santa Cruz Biotechnology, 1:1000), Sox-2 (#sc-365823, Santa Cruz Biotechnology, 1:1000), and peroxidase-conjugated β-Actin (#A3854, Sigma-Aldrich®, 1:25000). Membranes were blocked with 5% milk powder in Tris-Buffered Saline with Tween (TBS-T) before primary antibody incubation overnight, at 4°C with shaking. After three washes with TBS-T, HRP conjugated secondary antibodies [Donkey anti-Goat (#A16005, Invitrogen™, 1:5000) or Goat anti-Mouse (#554002, BD Pharmingen™, 1:5000)] was incubated for 1 h at room temperature (RT). Protein expression was detected by chemiluminescence using Amersham™ ECL™ Prime kit (#RPN2232, Cytiva) in a Bio-rad ChemiDoc Imaging System.

Immunocytochemistry

hiPSCs grown on laminin-coated coverslips were fixed for 15 min with 4% paraformaldehyde (PFA, #043368.9M, Thermo Scientific Chemicals), permeabilized with 0.2% Triton X-100 (TX-100, #T9284-100, Sigma-Aldrich®) in Phosphate-buffered saline (PBS) for 10 min, followed by 1 h blocking with 10% donkey serum (DS, #S30-100ML, Sigma-Aldrich®) in PBS at RT. Stem cells were then incubated for 2 h with primary antibodies OCT3/4 (#sc-5279, Santa Cruz Biotechnology, 1:100), SOX-2 (#sc-365823, Santa Cruz, 1:100), or Nanog (#sc-293121, Santa Cruz Biotechnology, 1:50) at 4°C overnight in blocking solution.

hiPSC-RPE was fixed either with methanol for 15 min on ice (for Claudin-19 and ZO-1 staining) or 4% PFA at RT (for phalloidin staining). Then, cells were permeabilized and blocked with perblock solution (0.05% Triton X-100 and 10% DS in PBS) for 1 h at RT. Cells were incubated with primary antibodies Claudin-19 (#365967, Santa Cruz Biotechnology, 1:100), ZO-1 (#40–2300, Invitrogen™, 1:100), or Alexa Fluor™ 568 Phalloidin F-actin probe (#A12380, Invitrogen™, 1:100) for 2 h at RT in perblock solution.

After washing cells with PBS, hiPSC or hiPSC-RPE was incubated for 1 h with secondary antibodies anti-Mouse or anti-Rabbit (#A-21202 and #A-21206, respectively, Invitrogen™, 1:500), followed by 5 min with DAPI (#D9542-5MG, Sigma-Aldrich®, 1:10 000). Coverslips were mounted with VECTASHIELD® Antifade Mounting Medium (#H-1000-10, Vector laboratories) and images were acquired with LSM980 (Zeiss) confocal microscope.

Brightfield images of hiPSC colonies, EBs, and ROs at different developmental stages (from d3 to d140 with PR development) were acquired using an EVOS™ XL Core digital microscope.

Phagocytosis assay

Porcine POS were isolated as described previously,[17] covalently labeled with Alexa Fluor 488 (A488), and stored at −80°C. Labeled POS were defrosted and washed with PBS by three centrifugation rounds of 10 min, at 5000 rpm, at 4°C. After each centrifugation, POS-A488 were resuspended in 1 mL sterile PBS, and kept with limited light exposure for a maximum of one week. Before RPE cell feeding, POS were sonicated three times for 5 min. hiPSC-RPE were incubated overnight with a 10% POS-A488 preparation diluted in X-VIVO, in a 5% CO_2 incubator at 37°C. The next day, cells were fixed and stained with phalloidin, as described in the previous section.

Transepithelial electrical resistance

hiPSC-RPE cultures from RBi CHM+ and RBi CHM– lines were plated onto laminin-coated transwell inserts (#3460, Corning®) at a density of $\sim 1x10^5$ cells cm^{-2}. X-VIVO medium was changed twice per week before measurements for 35d. TEER was measured using the EVOM™ epithelial volt-ohmmeter (#EVM-MT-03-01, World precision instruments). Data were represented using a 4-parameter logistic regression with 95% confidence intervals (CI).

Transmission electron microscopy (TEM)

All reagents and materials were purchased from Electron Microscopy Sciences, unless otherwise stated. Cells on glass coverslips were fixed in 2% PFA, and 2% glutaraldehyde in 0.1M phosphate buffer (PB) at pH 7.4 overnight at 4°C. After washing with PB, specimens were postfixed with 1% osmium tetroxide and 1.5% potassium ferrocyanide in distilled water for 1 h on ice, and then incubated with 1% tannic acid for 30 min at RT. Specimens were subsequently dehydrated with a series of increasing ethanol concentrations (50%, 70%, 90%, and 2 × 100%) before infiltrating and embedding in Epon resin (EMbed 812). After polymerizing at 65°C overnight, resin blocks were sectioned at 60–70 nm using a Reichart Ultracut S ultramicrotome (Leica) and a diamond knife (Diatome), and sections collected on copper mesh grids. Sections on grids were poststained with uranyl acetate and Reynold's lead citrate and imaged using a Hitachi H-7650 TEM equipped with an AMT XR41 M digital camera.

Quantitative PCR analysis

mRNA from hiPSC, hiPSC-RPE, or EBs (pool of 5) was extracted using RNeasy Mini Kit (#74104, Quiagen), according to manufacturer's instructions. Next, 1 μg of purified mRNA was reverse transcribed into cDNA using SuperScript™ II Reverse Transcriptase (#18064022, Invitrogen™). Reverse transcriptase quantitative polymerase chain reaction (RT-qPCR) was carried out in a QuantStudio™ 5 system (Applied Biosystems™) using PowerUp™ SYBR™ Green Master Mix (#A25742, Applied Biosystems™), following manufacturer's instructions. The primer pairs (forward/reverse) used are described in Table 1 and relative gene expression results were analyzed using $2^{-\Delta\Delta Ct}$ method,[18] normalized to the housekeeping gene *ACTB* levels.

Karyotyping

hiPSC colonies at 60–80% confluency were incubated with 0.1 μg/mL KaryoMAX™ Colcemid™ (#15212012, Gibco™) for 1:30–2 h before collection using TrypLE. The suspension was centrifuged, and the pellet was treated with

Table 1. Human Primer Sequences Used in RT-qPCR

Primer	*Sequence 5'–3'-Forward*	*Sequence 5'–3'-Reverse*
OCT4	CAGTGCCCGAAACCCACAC	GGAGACCCAGCAGCCTCAAA
SOX2	GGGAAATGGGAGGGGTGCAAAAGAGG	TTGCGTGAGTGTGGATGGGATTGGTG
NANOG	CAGAAGGCCTCAGCACCTAC	ATTGTTCCAGGTCTGGTTGC
KLF4-1	CCCACACTTGTGATTACGC	GGTAAGGTTTCTCACCTGTG
KLF4-2	TCTCCAATTCGCTGACCCAT	CGGATCGGATAGGTGAAGCT
ACTB	GAAGATCAAGATCATTGCTCCTC	ATCCACATCTGCTGGAAGG
RBP3	TCTGCTGGACAAGATCTACAG	TAGCGTTCACCTACAACCT
BEST1	GCAAGCAGGCTTTATGACTC	ATTGACAGGTTGGCAAACC
RPE65	AAGATGATGGTGTAGTTCTGAG	TGGCATTCAGAATCAGGAG
PMEL	ATCATCAATGGGAGCCAGG	ACCATCAGGGAAGATGCAG
MITF	CGTCCTGTATGCAGATGGA	CATCAAGCCCAAGATTTCCTC
TYRP1	ACACAGTGGAAGGTTACAG	GGAATAGATGAGCCAAATTGTG
MART1	ACTGTGAACCTGTGGTTCC	TGGTGACTGTTCTGCAGAG
TYR	TATCTACAAGATTCAGACCCAGAC	CCATGACCAGATCCGACTC
DCT	ATCTCCAGCGACTCATTGG	ACACATCACACTCGTTCCT
PAX6	GGGCGGAGTTATGATACCTACA	ATATCAGGTTCACTTCCGGGAA
OTX	TACGCCCTCCTCTTCCTACT	GCATGTGGGTGGTGATGATG
SOX1	CACCCGGATTACAAGTACC	ACTTGTCCTTCTTGAGCAG
GATA2	ACCTGTTGTGCAAATTGTCAGA	ATCCCTTCCTTCTTCATGGTCA
TBXT	CTGCTTATCAGAACGAGGAG	GTGATCACTTCTTTCCTTTGC
SOX7	ACTCCACTCCAACCTCCAAG	TTCATTGCGATCCATGTCCC
SOX17	ATCGGGGACATGAAGGTGAA	TCCTTAGCCCACACCATGAA
GATA4	AGATGCGTCCCATCAAGAC	CTGACTGAGAACGTCTGGG

RT-qPCR, Reverse transcriptase quantitative polymerase chain reaction

prewarmed 75 mM KCl hypotonic solution for 20 min at 37°C. Then, cells were fixed using a methanol-acetic acid solution at a 3:1 ratio followed by three 15 min centrifugations at 1250 rpm until the solution became translucid with a white pellet. G-banding at 400–550 band resolution was used to assess hiPSC genome integrity, with at least 20 metaphase spreads examined (Genomed, Lisbon, Portugal).

Statistical analysis

Data were analyzed using GraphPad Prism 9 software and is presented as mean ± SEM from at least $n = 3$ independent experiments, except otherwise noted. Student's *t-test* was used to compare groups of isogenic cell lines (RBi and Pt pairs were analyzed independently).

Results

Generation and characterization of CHM and control isogenic hiPSCs

In this work, we used two strategies to develop isogenic hiPSC lines to model CHM disease. In Strategy 1, we used a healthy donor cell line RBi001-A (henceforth named RBi CHM+) to produce a CHM mutant line targeting *CHM* exon 6 (RBi CHM−). Sequencing of the selected clone from the RBi CHM− mutant line confirmed the insertion of a C on nucleotide 809 ($CHM^{c.809insC}$), resulting in a frameshift mutation (Fig. 1A). In Strategy 2, in addition to the single-guide RNA (sgRNA), we supplied a single-stranded oligodeoxynucleotide (ssODN) template containing the corrected *CHM* sequence to promote homology-directed repair (HDR) in a CHM patient line (henceforth named Pt CHM−). In this study, we observed that the $CHM^{c.808C>T}$ mutation present in the Pt CHM− line was restored to a C in the selected Pt CHM+ clone (Fig. 1A). Moreover, we confirmed that all four cell lines used in this study presented a normal male karyotype (46, XY), with no chromosomal alteration (Fig. 1B).

Next, we analyzed the morphology and expression of pluripotency markers in the generated lines. All hiPSC lines exhibited typical pluripotent stem cell morphology (Fig. 2A), and expression of the pluripotency markers Oct-3/4, Nanog, and Sox-2 (Fig. 2B, D). Similarly, we observed that the mRNA expression of stemness markers (*OCT4, SOX2, NANOG,* and *KLF4*) was comparable in isogenic pairs (Fig. 2C). As expected, REP1 protein was absent in RBi CHM− and was restored to normal levels in Pt CHM+ after mutation correction (Fig. 2D).

REP1 deficiency in humans leads to a retinal exclusive phenotype, due to the activity of its isoform REP2 in remaining tissues, which is encoded by the CHM-like (*CHML*) gene and shares 75% similarity with *CHM*.[6,7] Both proteins are ubiquitously expressed; however, some Rabs in the retina have a binding preference for REP1, which REP2 cannot compensate for.[6,19] The sgRNAs were specifically designed to target the *CHM* gene only, and REP2 expression was not altered on either of the engineered cells (Fig. 2D).

hiPSC CHM isogenic lines recapitulate key RPE features

CHM pathophysiology is complex, affecting three interdependent retinal layers (choroid, photoreceptors [PRs], and RPE), with the RPE playing a critical role in disease progression.[6] RPE cells provide crucial support to the PRs by providing nutrients and performing POS phagocytosis, among other functions.[9,10] Considering the importance of the RPE for CHM progression, we evaluated the capacity of our newly developed cell lines to acquire an RPE phenotype.

We were able to successfully differentiate the four hiPSC lines into RPE, which exhibited the typical polygonal morphology and polarization, as shown by the expression of the tight junction markers Zonula Occludens-1 (ZO-1) and Claudin-19 at the interface between adjacent cells (Fig. 3A). Polarization between apical and basolateral membranes was confirmed by measuring the TEER of one of the hiPSC-RPE pairs, with RBi CHM+ reaching a predicted value of 285.2 $\Omega\ cm^{-2}$ (231.9, 384.7) and RBi CHM− reaching 192.0 $\Omega\ cm^{-2}$ (159.4, 231.6), considering a 95% CI (Fig. 3C).

We confirmed that the expression of pluripotent markers in hiPSC-RPE is greatly reduced (Fig. 3D, E), compared to RPE-specific genes (*RBP3, RPE65,* and *BEST1*), which are highly expressed (Fig. 3D). Of note, REP2 protein expression was decreased in hiPSC-RPE, when compared to their undifferentiated counterparts (Fig. 3E). Furthermore, we fed hiPSC-RPE with porcine POS-A488 overnight and confirmed that all cell lines were able to phagocytose the fluorescently labeled POS (Fig. 3B).

Another hallmark of RPE cells is the presence of melanin pigment, and using transmission electron microscopy (TEM), we could observe vesicles of all (eu)melanogenesis stages, including stage I to stage IV melanosomes, in all the cell lines studied (Fig. 4A). Interestingly, when subculturing our hiPSC-RPE, we observed that cells lacking *CHM* have significantly less pigment (Fig. 4B). Therefore, we investigated if genes involved in melanogenesis were differentially expressed in cells with and without the mutated *CHM* gene. We found that *MITF*, *MART-1*, and *TYR* mRNA transcript expression decreased significantly in Pt CHM− RPE cells when compared to the Pt CHM+ line, suggesting an impairment in the pigmentation machinery caused by REP1 loss (Fig. 4C). Although the amount of pigment is reduced, the molecular and cellular machinery required for complete melanin formation is present in all lines (Fig. 4A).

Embryoid bodies and retinal organoids obtained from hiPSC CHM isogenic lines

To explore the potential of the hiPSC CHM lines to recapitulate the self-organization of early embryogenesis, the four hiPSC lines were differentiated into embryoid bodies (EBs) and retinal organoids (ROs). During EB formation, no morphological change was detected between EBs derived from hiPSCs lacking *CHM* (RBi CHM− and Pt CHM−), compared to those with *CHM* (RBi CHM+ and Pt CHM+, Fig. 5A). Moreover, on day 7 (d7), the two pairs of isogenic EBs expressed specific genes related with endodermal (*PAX6, OTX1,* and *SOX1*), mesodermal (*GATA2* and *TBXT*), and ectodermal (*SOX7, SOX17,* and *GATA4*) lineages, showing no significant difference within isogenic pairs (Fig. 5B). On

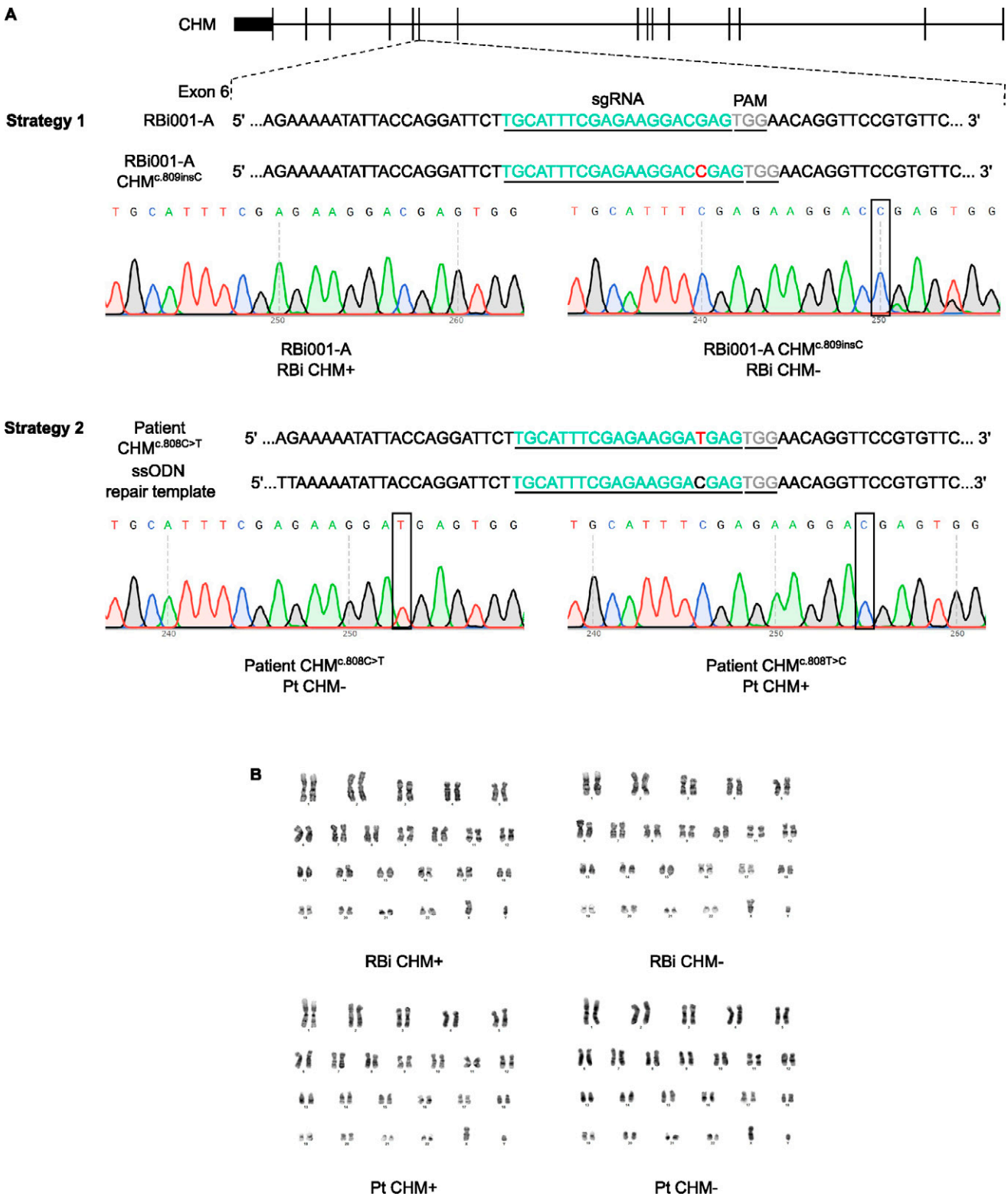

FIG. 1. CRISPR/Cas9 strategies to generate isogenic hiPSC lines to model CHM disease. **(A)** Schematic representation of the two strategies. Strategy 1 was designed to generate a CHM KO cell line isogenic of RBi001-A (named RBi CHM+). The resulting frameshift mutation in RBi CHM− is highlighted, with a C insertion on position 809. Strategy 2 was used to produce a Pt CHM− isogenic cell line. Here, the donor template is represented alongside the Pt CHM− sequence, with the T mutation and repaired C nucleotide emphasized. sgRNA and Protospacer Adjacent Motif sequences are indicated in green and gray, respectively, and mutated nucleotides in red. Corresponding Sanger sequencing of the mutation sites is shown for each line and strategy. **(B)** Representative G-banding of all four cell lines, showing normal male (46, XY) karyotype. CHM, Choroideremia; sgRNA, single guide RNAs.

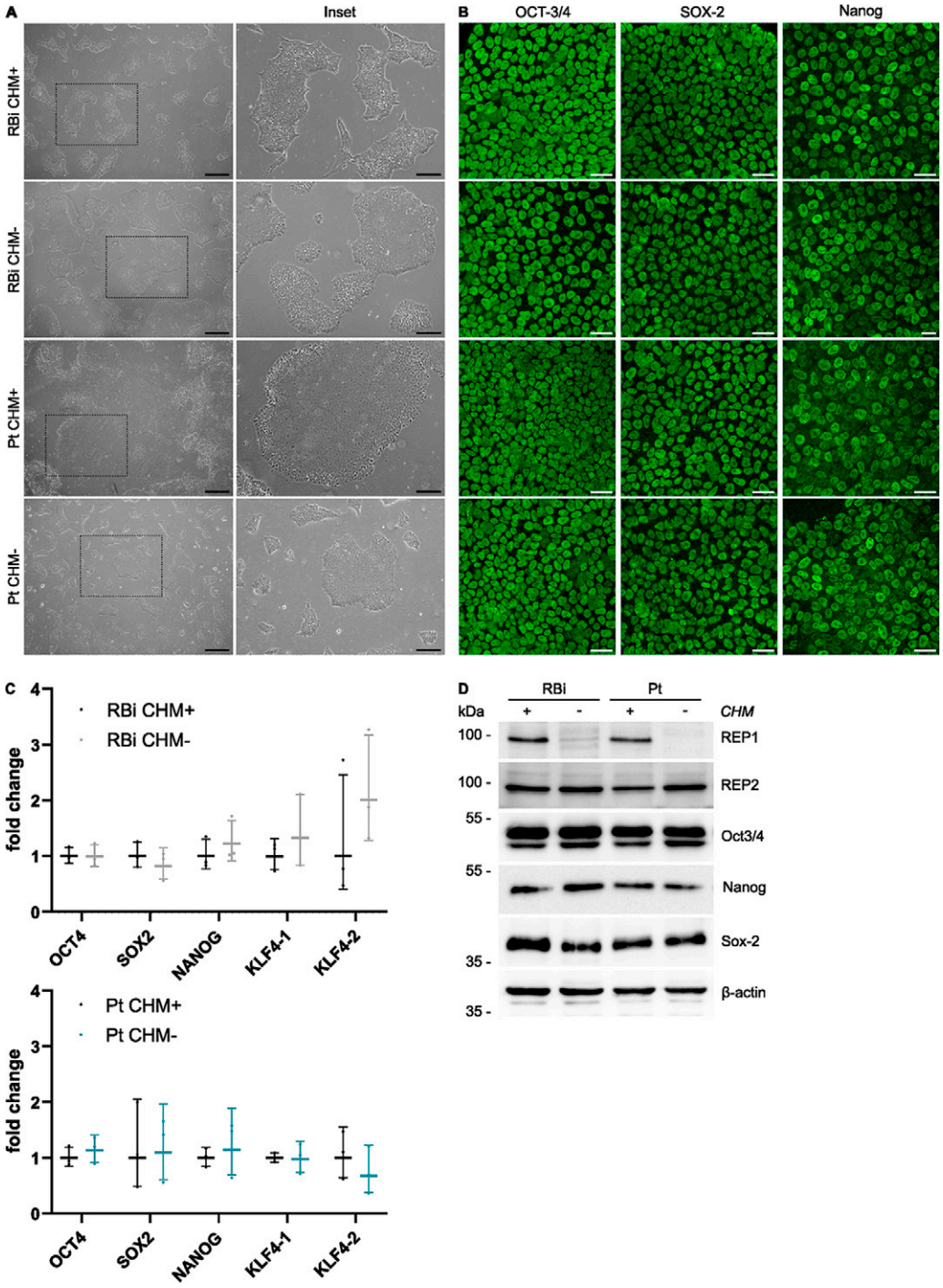

FIG. 2. Characterization of the engineered CHM hiPSC lines. **(A)** Brightfield images of each hiPSC line, with colonies highlighted on the right (Scale bar 500 μm, inset 200 μm). Expression of pluripotency markers was detected by **(B)** immunocytochemistry (scale bar 30 μm), **(C)** RT-qPCR gene relative expression, represented using geometric mean ± geometric SD of $n = 3$ independent experiments, Student's *t test* not significant (RBi pair p-values: OCT4 0.99; SOX2 0.45; NANOG 0.44; KLF4-1 0.38; KLF4-2 0.41; Pt pair p-values: OCT4 0.45; SOX2 0.95; NANOG 0.52; KLF4-1 0.99; KLF4-2 0.43); and **(D)** WB analysis from $n = 2$ independent experiments, confirming pluripotency maintenance after genetic engineering. WB shows the absence of REP1 protein in RBi CHM– and Pt CHM– lines and normal expression of REP2 in all cell lines. CHM, Choroideremia; REP1, Rab escort protein 1; RT-qPCR, Reverse transcriptase quantitative polymerase chain reaction.

differentiation d140, ROs presented prominent PRs located at the surface (Fig. 5A) in all lines.

Discussion

The complex pathophysiology of the CHM degenerative process involves the interaction between the RPE, choroid, and PRs, and depends heavily on RPE cells.[6] The aim of this work was to generate new cellular models to study the RPE in the context of CHM pathology, taking advantage of hiPSCs and CRISPR/Cas9 technology to develop isogenic models of the disease. In the long term, we believe that these models constitute a powerful platform to delve into the mechanisms of RPE degeneration in CHM, as well as other diseases of the RPE, which are still unclear.

The RPE is thought to be one of the primary sites of degeneration in CHM, being situated between the PRs and choroid.[6] Therefore, to accurately model CHM cellular phenotypes, we derived our newly developed hiPSCs into RPE and show that these cells reproduce key RPE features. These include the expression of tight junction markers ZO-1 and Claudin-19, demonstrating the typical RPE polygonal morphology, along with polarization, as shown by the TEER increase from 20d of differentiation onwards, observed for the RBi CHM pair. Moreover, all hiPSC-RPE express RPE-specific genes, as well as melanosomes in all stages of melanosome maturation, and have the capacity to phagocytose POS.

REP1 participates in the prenylation of Rab GTPases, a post-translational modification catalyzed by Rab geranylgeranyltransferase type II (also called GGTase-II) and required for proper cellular localization, membrane association, and protein–protein interactions of Rabs.[20] Rab proteins are involved in intracellular vesicle trafficking, making REP1 essential for this process, particularly for melanosome trafficking.[21] We observed that hiPSC-RPE lacking REP1 have less pigment than their control counterparts to the naked eye, and therefore we explored the possibility of a pigmentation deficiency in these cells. Indeed, some genes of the melanogenesis pathway are decreased in the Pt CHM− line, compared to the isogenic control Pt CHM+. Although no difference was observed in melanin formation by electron microscopy, and all stages of melanosome vesicles were present, the decreased expression of melanogenesis genes is in line with findings in zebrafish CHM mutant models (*chm*^{ru848}), which have a reduction of *tyr, tryp1a, mitf, dct,* and *pmel* at 4 days postfertilization (dpf).[21,22] Because they lack the REP2 paralog, these fish have a more severe phenotype with systemic degeneration and on average do not survive past 5dpf. Moreover, other pigmentary disturbances were observed in these fish at 4dpf, including lack of melanosomes in the choroid and reduction in choroidal blood vessel and interstitial pillar diameter, along with a total melanin decrease.[21,22]

Following synthesis, Rab proteins are escorted either by REP1 or its paralog REP2, presenting them to GGTase-II for prenylation. Subsequently, Rabs are inserted in their target membranes and activated, where they can perform their functions in membrane trafficking, vesicle formation, movement, and fusion. While REP2 also supports Rab prenylation, it does so with a different specificity than REP1. Rab proteins are of particular importance in the retina since they are involved in POS phagocytosis and trafficking of melanosomes to apical microvilli, contributing to RPE homeostasis. Hence, mutations that affect REP1 lead to a prenylation deficit, disrupting these pathways, a characteristic of CHM pathogenesis.[20]

Interestingly, in our hiPSC-RPE models, we observed that REP2 protein expression decreased after RPE differentiation when compared to their undifferentiated counterparts. In agreement, Fry and colleagues, by using fibroblasts from CHM patients, mention that a higher protein loading was necessary for REP2 detection.[20] This observation hints at a possible lower REP2 expression when compared to REP1, which could be more noticeable in fully differentiated RPE cells than in fibroblasts. Altogether, these data suggest that the inability of REP2 to compensate for the loss of REP1 in CHM could be due to a combination of lower expression and Rab GTPase substrate specificity, resulting in a primary eye phenotype.[7,20]

Finally, we show that these new hiPSC CHM isogenic models can differentiate into EBs, suggesting they are able to replicate the self-organization of early embryogenesis. The EBs formed express typical markers from the endodermal, mesodermal, and ectodermal lineages. Differentiation was further directed into ROs, which are becoming potent models for investigating retinal development and illnesses, as well as toxicology, and novel treatments for retinal diseases.[23] These 3D models are extremely valuable because they are also derived from hiPSCs and can be obtained from individuals suffering from specific disorders. ROs have the advantage of forming a 3D structure, mimicking all neuroretina cell types, including Müller cells and astrocytes, similar to the human retina.[23] Importantly, we observe that the organoids formed using our model cells develop PRs,

FIG. 3. hiPSC CHM lines can be successfully differentiated into RPE. **(A)** Immunofluorescence images of tight junction markers Claudin-19 and ZO-1 after differentiation (scale bar 20 μm, inset 10 μm). **(B)** Demonstration of the phagocytosis capacity of hiPSC-RPE (scale bar 10 μm, inset 5 μm). **(C)** TEER measurements of RBi CHM+ and CHM-hiPSC-RPE from d5 to d35 of differentiation. $n = 1$ differentiation, with 3 replicate measurements. Data were represented using a 4-parameter logistic regression with 95% CI. **(D)** Downregulation of pluripotent markers (*OCT4, NANOG,* and *SOX2*) and upregulation of RPE-specific genes (*RBP3, BEST1,* and *RPE65*) in hiPSC-RPE. mRNA expression levels are represented as $\log_2$ fold change relative to RBi CHM+ or Pt CHM+ undifferentiated cells, respectively. Data from $n = 3$ independent experiments represented as mean ± SEM. **(E)** Comparative analysis between undifferentiated and differentiated states of various cell lines, showing a reduction of pluripotent specific proteins in hiPSC-RPE, absence or presence of REP1 in the edited cell lines, and REP2 presence in all lines. CHM, Choroideremia; hiPSC, human induced pluripotent stem cells; REP1, Rab escort protein 1; RPE, retinal pigment epithelium; TEER, transepithelial electrical resistance.

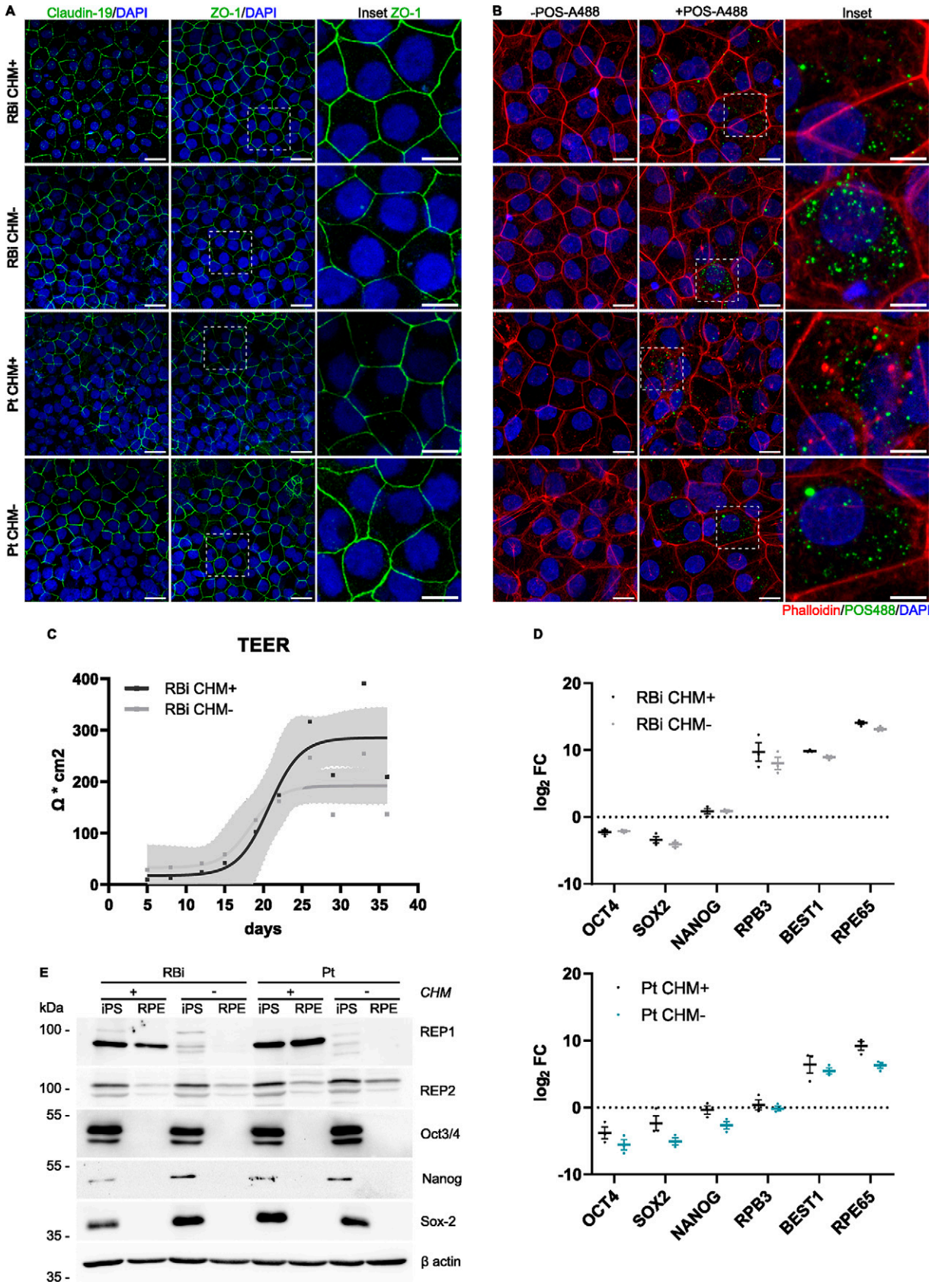
A
Claudin-19/DAPI
ZO-1/DAPI
Inset ZO-1
RBi CHM+
RBi CHM-
Pt CHM+
Pt CHM-
B
-POS-A488
+POS-A488
Inset
Phalloidin/POS488/DAPI
C
TEER
RBi CHM+
RBi CHM-
Ω * cm2
days
D
RBi CHM+
RBi CHM-
log2 FC
OCT4
SOX2
NANOG
RPB3
BEST1
RPE65
Pt CHM+
Pt CHM-
E
RBi
Pt
CHM
kDa
iPS
RPE
REP1
REP2
Oct3/4
Nanog
Sox-2
β actin

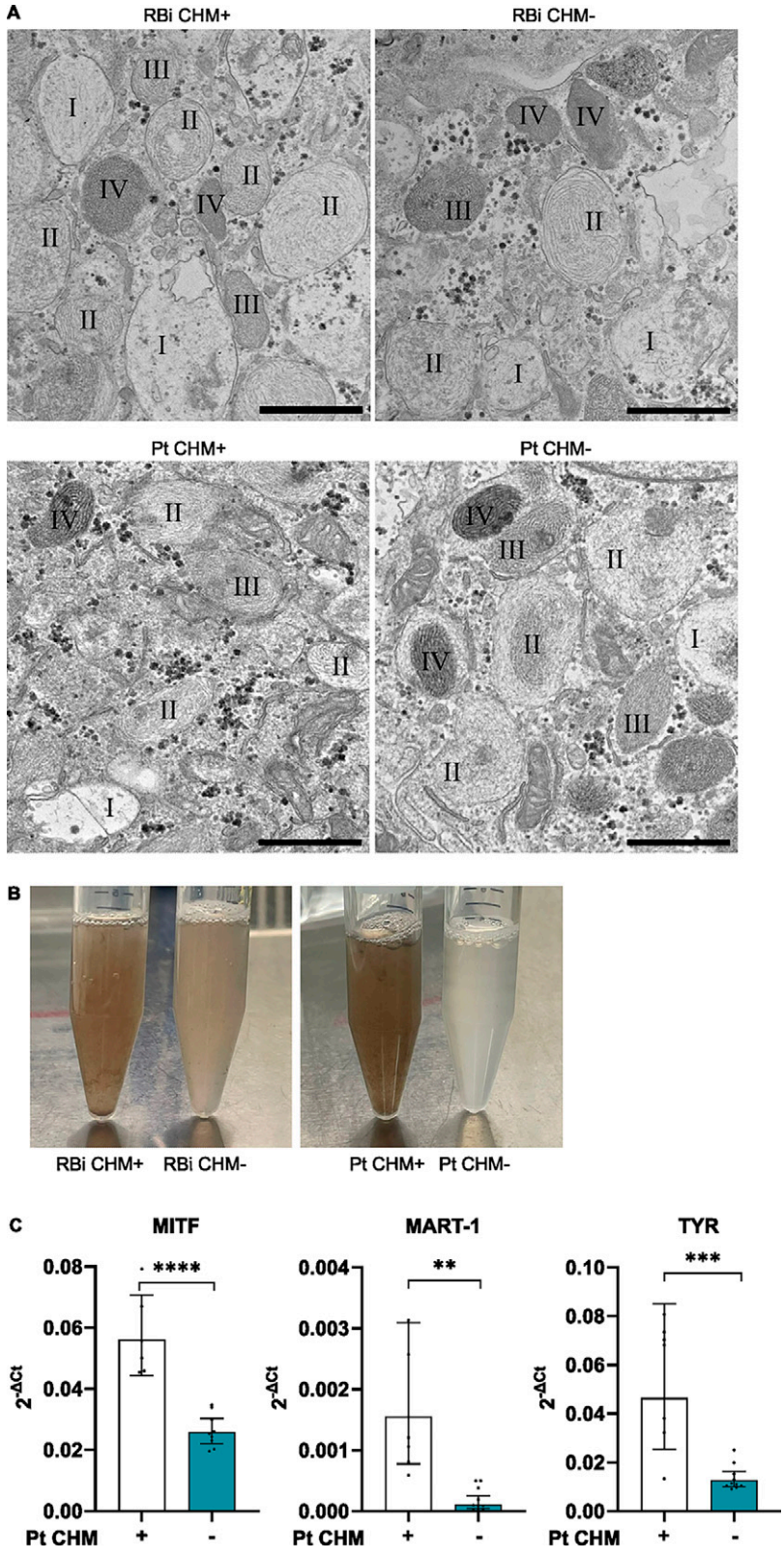

FIG. 4. Pigmentation appears to be differentially expressed between healthy and CHM lines. **(A)** TEM images of examples of all stages of (eu)melanogenesis, including stage I to stage IV melanosomes (as labeled), in both control and CHM hiPSC-RPE cells (scale bar 1 μm). **(B)** RBi CHM− and Pt CHM− cells have less pigment in suspension, photo taken during cell passing from P1 to P2. **(C)** *$p < 0.05$ RPE from Pt CHM− cells have a slight decrease in mRNA expression of pigmentation genes (*MITF, MART-1,* and *TYR*), data representative of $n = 3$ for Pt CHM+ and Pt CHM− lines. CHM, Choroideremia; hiPSC, human induced pluripotent stem cells; REP1, Rab escort protein 1; RPE, retinal pigment epithelium.

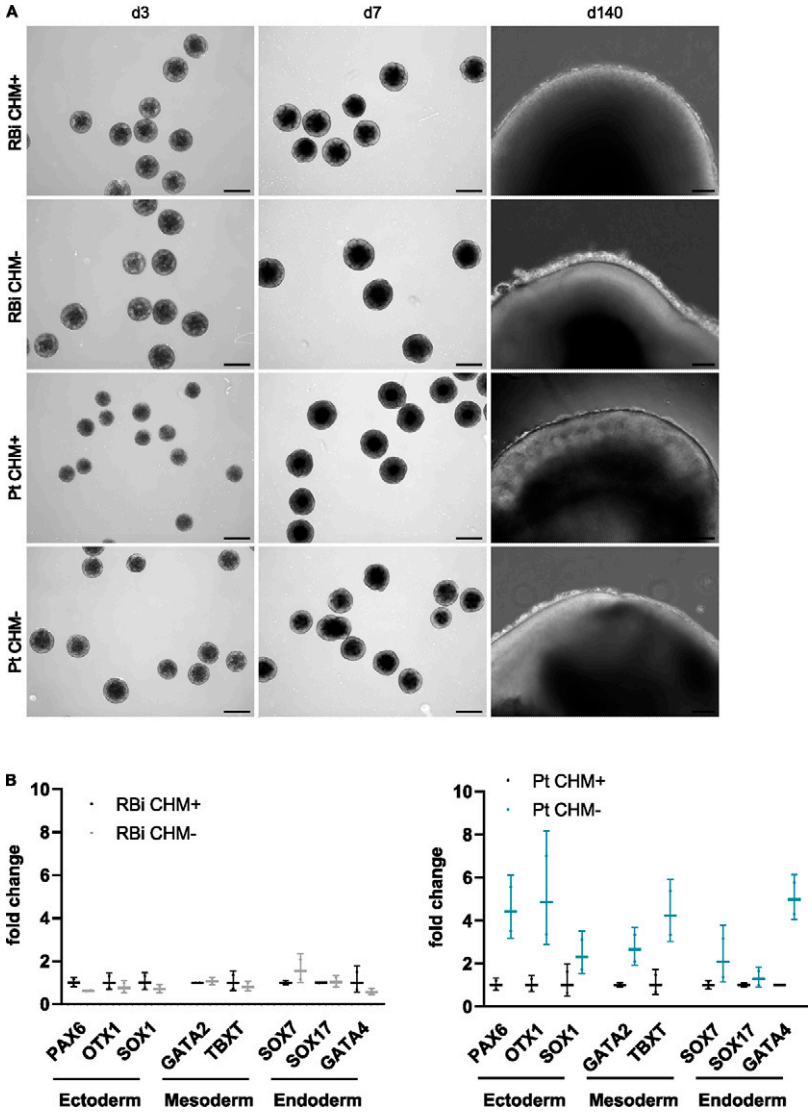

FIG. 5. hiPSC CHM lines can effectively form EBs and differentiate into ROs. **(A)** Brightfield images of EBs on d3 and d7 and PRs in the outer layer of ROs on d140. **(B)** Relative gene expression analysis of EBs derived from the four cell lines on d7. EBs expressed the specific markers of different embryonic cell lineages, *PAX6, OTX1,* and *SOX1* (endoderm); *GATA2* and *TBXT* (mesoderm); and *SOX7, SOX17,* and *GATA4* (ectoderm). Data represented as geometric mean ± geometric SD from $n = 2$ independent RO differentiations. CHM, Choroideremia; EBs, embryoid bodies; hiPSC, human induced pluripotent stem cells; ROs, retinal organoids.

known to be both photosensitive and phototransductive, enabling diverse types of studies such as advanced electrophysiology.[23]

In conclusion, we developed pairs of isogenic hiPSC CHM lines representing new models, which can now be used to further explore the intricate mechanisms of retinal degeneration of this blinding disease.

Acknowledgments

The authors are grateful to David Gamm Lab (Wisconsin University) for the gift of a CHM male patient-derived hiPSC line CRFi001-A, and the Molecular Mechanisms of Disease Lab, the Ocular Low-Cost Gene Therapy Lab, and the Degeneration and Aging Lab for their advice and support. The authors thank the Cell Culture facility at NOVA Medical School (NMS), the scientific and technical assistance of T. Pereira from the NMS Microscopy facility. They thank the Electron Microscopy Facility at Instituto Gulbenkian de Ciência. They also acknowledge the local slaughterhouse (CASO — Centro de Abate de Suínos do Oeste) that generously provided porcine eyes.

Author Disclosure Statement

The authors state that the research was conducted without any commercial or financial relationship that could be regarded as a potential conflict of interests.

Funding Information

The authors declare financial support was received for the research, authorship, and/or publication of this article. Research was supported by Fundação para a Ciência e Tecnologia (FCT)—Portugal (including iNOVA4Health projects UIDB/04462/2020, UIDP/04462/2020, and associated laboratory LS4FUTURE with reference LA/P/0087/2020). A.F.F. is funded by FCT PhD studentship (2022.12254.BD). M.L.S. is funded by the individual grant CEECIND/01536/2018. A.S.F. postdoctoral contract is funded by "La Caixa Foundation" (NASCENT HR22-00569). P.A. is supported by grant EXPL/MED-OUT/0599/2021, funded by national funds from FCT/MCTES, and individual grant CEECIND/03862/2020. L.L. is a recipient of a Choroideremia Research Foundation postdoctoral fellowship, Throssell-Hillier Research Award. Research at the Center for the Unknown is supported by Fundação Champalimaud.

References

1. Seabra MC. New insights into the pathogenesis of choroideremia: A tale of two REPs. Ophthalmic Genet 1996;17: 43–46; doi: 10.3109/13816819609057869
2. Gordiyenko NV, Fariss RN, Zhi C, et al. Silencing of the CHM Gene Alters Phagocytic and Secretory Pathways in the Retinal Pigment Epithelium. Invest Ophthalmol Vis Sci 2010;51:1143–1150; doi: 10.1167/iovs.09-4117
3. Seabra MC, Ho YK, Anant JS. Deficient geranylgeranylation of Ram/Rab27 in choroideremia. J Biol Chem 1995; 270:24420–24427; doi: 10.1074/jbc.270.41.24420
4. Seabra MC, Mules EH, Hume AN. Rab GTPases, intracellular traffic and disease. Trends Mol Med 2002;8:23–30; doi: 10.1016/s1471-4914(01)02227-4
5. Tolmachova T, Anders R, Abrink M, et al. Independent degeneration of photoreceptors and retinal pigment epithelium in conditional knockout mouse models of choroideremia. J Clin Invest 2006;116:386–394; doi: 10.1172/JCI26617
6. Tolmachova T, Wavre-Shapton ST, Barnard AR, et al. Retinal Pigment Epithelium Defects Accelerate Photoreceptor Degeneration in Cell Type–Specific Knockout Mouse Models of Choroideremia. Invest Ophthalmol Vis Sci 2010;51: 4913–4920; doi: 10.1167/iovs.09-4892
7. Sarkar H, Moosajee M. Choroideremia: Molecular mechanisms and therapies. Trends Mol Med 2022;28:378–387.
8. Cremers FP, Armstrong SA, Seabra MC, et al. REP-2, a Rab escort protein encoded by the choroideremia-like gene. J Biol Chem 1994;269:2111–2117.
9. Wavre-Shapton ST, Tolmachova T, da Silva ML, et al. Conditional Ablation of the Choroideremia Gene Causes Age-Related Changes in Mouse Retinal Pigment Epithelium. PLoS One 2013;8:e57769.
10. Lakkaraju A, Umapathy A, Tan LX, et al. The cell biology of the retinal pigment epithelium. Prog Retin Eye Res 2020; 78:100846.
11. Foltz LP, Clegg DO. Rapid, Directed Differentiation of Retinal Pigment Epithelial Cells from Human Embryonic or Induced Pluripotent Stem Cells. J Vis Exp 2017; doi: 10 .3791/56274
12. Pfeffer BA, Fliesler SJ. Reassessing the suitability of ARPE-19 cells as a valid model of native RPE biology. Exp Eye Res 2022;219:109046.
13. Hazim RA, Volland S, Yen A, et al. Rapid differentiation of the human RPE cell line, ARPE-19, induced by nicotinamide. Exp Eye Res 2019;179:18–24.
14. Markert EK, Klein H, Viollet C, et al. Transcriptional comparison of adult human primary Retinal Pigment Epithelium, human pluripotent stem cell-derived Retinal Pigment Epithelium, and ARPE19 cells. Front Cell Dev Biol 2022; 10:910040.
15. Bassett AR. Editing the genome of hiPSC with CRISPR/-Cas9: Disease models. Mamm Genome 2017;28:348–364.
16. Capowski EE, Samimi K, Mayerl SJ, et al. Reproducibility and staging of 3D human retinal organoids across multiple pluripotent stem cell lines. Development 2019;146; doi: 10 .1242/DEV.171686/VIDEO-7
17. Parinot C, Rieu Q, Chatagnon J, et al. EF. Large-Scale Purification of Porcine or Bovine Photoreceptor Outer Segments for Phagocytosis Assays on Retinal Pigment Epithelial Cells. J Vis Exp 2014:52100.
18. Livak KJ, Schmittgen TD. Analysis of Relative Gene Expression Data Using Real-Time Quantitative PCR and the 2−ΔΔCT Method. Methods 2001;25:402–408.
19. Cunha DL, Richardson R, Tracey-White D, et al. REP1 deficiency causes systemic dysfunction of lipid metabolism and oxidative stress in choroideremia. JCI Insight 2021;6; doi: 10.1172/JCI.INSIGHT.146934
20. Fry LE, Patrício MI, Jolly JK, et al. Expression of Rab Prenylation Pathway Genes and Relation to Disease Progression in Choroideremia. Transl Vis Sci Technol 2021;10:12; doi: 10.1167/TVST.10.8.12
21. Sarkar H, Tracey-White D, Hagag AM, et al. Loss of REP1 impacts choroidal melanogenesis and vasculogenesis in choroideremia. Biochim Biophys Acta Mol Basis Dis 2024; 1870:166963.
22. Moosajee M, Tulloch M, Baron RA, et al. Single choroideremia Gene in Nonmammalian Vertebrates Explains Early Embryonic Lethality of the Zebrafish Model of Choroideremia. Invest Ophthalmol Vis Sci 2009;50:3009–3016.
23. L de L, Antas P, Ferreira IS, et al. 3D human retinal organoid model for the study of early diabetic retinopathy. bioRxiv 2023; doi: 10.1101/2023.09.04.556258

Address correspondence to:
Dr. Pedro Antas
NOVA Medical School Rua Câmara Pestana
n.°s 6
6-A e 6-B 1150-082 Lisboa PORTUGAL

E-mail: pedro.antas@nms.unl.pt

Received for publication June 7, 2024
Accepted after revision July 26, 2024
Prepublished on Liebert Instant Online July 30, 2024